Article

p-Channel Organic Semiconductors Based on Hybrid Acene–Thiophene Molecules for Thin-Film Transistor Applications

Jeffrey A. Merlo, Christopher R. Newman, Christopher P. Gerlach, Tommie W. Kelley, Dawn V. Muyres, Sandra E. Fritz, Michael F. Toney, and C. Daniel Frisbie

J. Am. Chem. Soc., **2005**, 127 (11), 3997-4009• DOI: 10.1021/ja044078h • Publication Date (Web): 01 March 2005

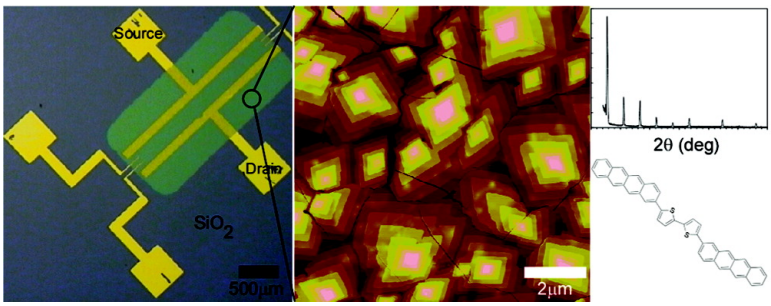

More About This Article

Additional resources and features associated with this article are available within the HTML version:

- Supporting Information
- Links to the 27 articles that cite this article, as of the time of this article download
- Access to high resolution figures
- Links to articles and content related to this article
- Copyright permission to reproduce figures and/or text from this article

View the Full Text HTML

J|A|C|S
ARTICLES
Published on Web 03/01/2005

p-Channel Organic Semiconductors Based on Hybrid Acene−Thiophene Molecules for Thin-Film Transistor Applications

Jeffrey A. Merlo,[†] Christopher R. Newman,[†] Christopher P. Gerlach,[‡] Tommie W. Kelley,[‡] Dawn V. Muyres,[‡] Sandra E. Fritz,[†] Michael F. Toney,[§] and C. Daniel Frisbie*,[†]

Contribution from the Department of Chemical Engineering and Materials Science, University of Minnesota, 421 Washington Avenue SE, Minneapolis, Minnesota 55455, 3M Company, Corporate Research Materials Laboratory, St. Paul, Minnesota 55144, and Stanford Synchrotron Radiation Laboratory, Stanford Linear Accelerator Center, 2575 Sand Hill Road, M/S 69, Menlo Park, California 94025

Received September 28, 2004; E-mail: frisbie@cems.umn.edu

Abstract: We report the structural and electrical characterization of two new p-channel organic semiconductors, 5,5′-bis(2-tetracenyl)-2,2′-bithiophene (**1**) and 5,5′-bis(2-anthracenyl)-2,2′-bithiophene (**2**). Both compounds exhibited a high degree of thermal stability with decomposition temperatures of 530 °C and 425 °C for **1** and **2**, respectively. The thin-film structures of **1** and **2** were examined using wide-angle X-ray diffraction (XRD), grazing incidence X-ray diffraction (GIXD), and atomic force microscopy (AFM). Films of **1** and **2** pack in similar triclinic unit cells with the long axes of the molecules nearly perpendicular to the substrate. Thin-film transistors (TFTs) based on **1** and **2** exhibit contact-corrected linear regime hole mobility as high as 0.5 cm^2/Vs and 0.1 cm^2/Vs, respectively. The specific contact resistance at high gate voltages for gold top contacts was 2×10^4 Ω cm and 3×10^4 Ω cm for 35 nm thick films of **1** and **2**, respectively. Long-term air stability tests revealed less degradation of the electrical properties of **1** and **2** in comparison to pentacene. Variable temperature measurements revealed activation energies as low as 22 and 27 meV for **1** and **2**, respectively. The temperature and gate voltage dependence of the mobility are discussed in terms of a double exponential distribution of trap states and a model accounting for the layered structure of the organic films. The enhanced air and thermal stability over pentacene, combined with good electrical performance characteristics, make **2** a promising candidate for future organic TFT applications.

1. Introduction

The acene and thiophene oligomers represent two of the most heavily studied series of compounds for use as organic semiconductors.[1−11] However, molecules that incorporate 2-anthracenyl[12] and 2-tetracenyl[13,14] fragments have not been widely studied for their semiconducting properties. Here we describe materials based on anthracene and tetracene units combined with thiophene oligomers, which constitute a new class of hybrid acene−thiophene organic semiconductors (see Scheme 1). These compounds are thermally stable, high melting point solids that can be sublimed readily to form high quality polycrystalline films.

Over the past few years, pentacene-based TFTs have been developed to the point that some of the key performance metrics (i.e., $\mu > 1$ cm^2/Vs, $I_{on}/I_{off} > 10^6$)[15,16] are acceptable for low level logic circuits and display applications. However, concerns regarding the commercial viability of pentacene devices center on its environmental instability (i.e., slow reaction with oxygen and water) and low solubility. The higher oxidation potentials of anthracenyl and tetracenyl fragments compared to pentacene are expected to stabilize **1** and **2** with respect to doping by oxygen (air-doping). Furthermore, certain substituted thiophene

[†] University of Minnesota.
[‡] 3M Company.
[§] Stanford Linear Accelerator Center.

(1) Newman, C. R.; Frisbie, C. D.; da Silva Filho, D. A.; Bredas, J.-L.; Ewbank, P. C.; Mann, K. R. *Chem. Mater.* **2004**, *16*, 4436−4451.
(2) Dimitrakopoulos, C. D.; Malenfant, P. R. L. *Adv. Mater.* **2002**, *14*, 99−117.
(3) Katz, H. E.; Bao, Z.; Gilat, S. L. *Acc. Chem. Res.* **2001**, *34*, 359−369.
(4) Katz, H. E.; Bao, Z. *J. Phys. Chem. B* **2000**, *104*, 671−678.
(5) Katz, H. E. *J. Mater. Chem.* **1997**, *7*, 369−376.
(6) Lovinger, A. J.; Rothberg, L. J. *J. Mater. Res.* **1996**, *11*, 1581−1592.
(7) Facchetti, A.; Mushrush, M.; Katz, H. E.; Marks, T. J. *Adv. Mater.* **2003**, *15*, 33−38.
(8) Hong, X. M.; Katz, H. E.; Lovinger, A. J.; Wang, B.-C.; Raghavachari, K. *Chem. Mater.* **2001**, *13*, 4686−4691.
(9) Sheraw, C. D.; Jackson, T. N.; Eaton, D. L.; Anthony, J. E. *Adv. Mater.* **2003**, *15*, 2009−2011.
(10) Lin, Y.-Y.; Gundlach, D. J.; Nelson, S. F.; Jackson, T. N. *IEEE Trans. Electron. Devices* **1997**, *44*, 1325−1331.
(11) Northrup, J. E.; Chabinyc, M. L. *Phys. Rev. B: Condens. Mater.* **2003**, *68*, 041202/1−4.
(12) Aleshin, A. N.; Lee, J. Y.; Chu, S. W.; Kim, J. S.; Park, Y. W. *Appl. Phys. Lett.* **2004**, *84*, 5383−5385.
(13) Gundlach, D. J.; Nichols, J. A.; Zhou, L.; Jackson, T. N. *Appl. Phys. Lett.* **2002**, *80*, 2925−2927.
(14) Kelley, T. W.; Baude, P. F.; Gerlach, C.; Ender, D. E.; Muyres, D.; Haase, M. A.; Vogel, D. E.; Theiss, S. D. *Chem. Mater.* **2004**, *16*, 4413−4422.
(15) Klauk, H.; Halik, M.; Zshieschang, U.; Schmid, G.; Radlik, W.; Weber, W. *J. Appl. Phys.* **2002**, *92*, 5259−5263.
(16) Sheraw, C. D.; Zhou, L.; Huang, J. R.; Gundlach, D. J.; Jackson, T. N.; Kane, M. G.; Hill, I. G.; Hammond, M. S.; Campi, J.; Greening, B. K.; Francl, J.; West, J. *Appl. Phys. Lett.* **2002**, *80*, 1088−1090.

Scheme 1. Chemical Structures of 5,5′-Bis(2-tetracenyl)-2,2′-bithiophene (**1**) and 5,5′-Bis(2-anthracenyl)-2,2′-bithiophene (**2**)

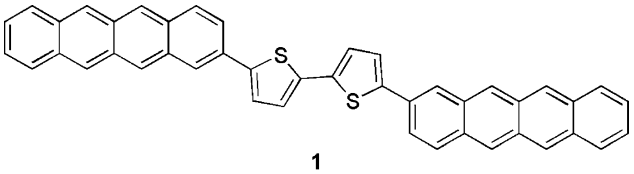

1

5,5'-bis-(2-tetracenyl)-2,2'-bithiophene

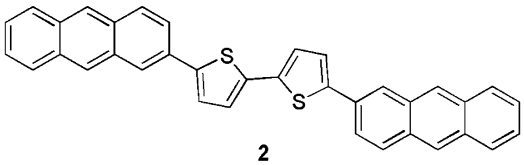

2

5,5'-bis-(2-anthracenyl)-2,2'-bithiophene

semiconductors[17−19] have shown good stability under ambient environmental conditions. We have used bithiophene linkers to extend the conjugation between acenyl fragments[20] and to open a strategy to increase the solubility (**1** and **2** are insoluble) by β-substitutions on the thiophene rings.

Here we report the structural and electrical characterization of two new p-channel organic semiconductors from this class of hybrid acene−thiophene materials, 5,5′-bis(2-tetracenyl)-2,2′-bithiophene (**1**) and 5,5′-bis(2-anthracenyl)-2,2′-bithiophene (**2**). These compounds exhibit remarkable thermal stability relative to other organic semiconductors as determined by differential scanning calorimetry (DSC), differential thermal analysis (DTA), and thermal gravimetric analysis (TGA). Using atomic force microscopy (AFM), X-ray diffraction (XRD), and grazing incidence X-ray diffraction (GIXD), we have determined the thin-film unit cell parameters, which are consistent with herringbone type packing. Importantly, electrical characterization revealed superior overall transistor performance (high mobility, large on/off current ratio, and increased air stability). In particular, the stability of transistors of **2** in air was found to be much better than pentacene. We have analyzed the hole mobility as a function of temperature and gate voltage and have estimated hole trap concentrations using a multiple trap and release (MTR) model. The modeling work reveals that a simple MTR picture is not adequate to describe transport, and it is likely necessary to consider the distribution of holes over the discrete layers of the semiconductor near the gate dielectric. We conclude by outlining a strategy for more realistic modeling of the electrical transport in layered crystalline organic semiconductors.

2. Experimental Methods

2.A. Synthesis and Purification. General. Stille coupling reactions were run under N_2. DMF was vacuum distilled from $MgSO_4$ and stored in a Straus flask. 1,4-Dioxane was anhydrous grade from Aldrich and used as received. 2-Bromoanthracene was synthesized by a Meerwein−Pondorf reduction of 2-bromoanthraquinone. The synthesis of 2-chlorotetracene[21] was carried out analogously. Both compounds may be purified by vacuum sublimation. ($Pd_2(dba)_3$) (dba = dibenzylideneacetone), ($Pd(PPh_3)_4$), tri-*tert*-butylphosphine (P(*t*-Bu)$_3$) (10 wt % in hexanes), and CsF were purchased from Strem Chemicals. CsF was ground to a fine powder, dried under vacuum at 100 °C for several hours, and stored in a drybox. 5,5′-Bis(tri-*n*-butylstannyl)-2,2′-bithiophene[22] was prepared according to a literature route.

5,5′-Bis(2-tetracenyl)-2,2′-bithiophene. The reaction to make **1** is shown in Scheme 2 below. A vessel was successively charged with $Pd_2(dba)_3$ (103 mg, 0.112 mmol, 1.5%), CsF (2.54 g, 16.7 mmol, 2.2 equiv), dioxane (120 mL), 2-chlorotetracene (2.00 g, 7.61 mmol), 5,5′-bis(tri-*n*-butylstannyl)-2,2′-bithiophene (2.83 g, 3.81 mmol), and P(*t*-Bu)$_3$ (1.3 mL, 0.45 mmol, 5.9 mol %) and heated at 100 °C for 36 h. The solid was isolated by filtration and successively washed with water (100 mL), 5% HCl (aq) (100 mL), and additional water. The crude material was purified by vacuum train sublimation ($P \approx 10^{-5}$ Torr) at a source temperature of 400−500 °C, to afford 1.25 g (53%) of deep red product. From the coolest zone, 0.33 g of 2-chlorotetracene starting material (17% on input) was recovered. LREIMS: calcd. for $C_{44}H_{26}S_2$ [M^+], 618.1476; found, 618.2. DSC (20 °C/min): 533 °C (mp, ΔH = 183 J g^{-1}). Anal. Calcd for $C_{44}H_{26}S_2$: C, 85.4%; H, 4.23%; S, 10.3%. Found: C, 84.6%; H, 4.25%.

5,5′-Bis(2-anthracenyl)-2,2′-bithiophene. The reaction to make **2** is shown in Scheme 3 below. A vessel was loaded with 5,5′-bis(tri-*n*-butylstannyl)-2,2′-bithiophene (3.16 g, 4.25 mmol), DMF (40 mL), 2-bromoanthracene (2.19 g, 8.50 mmol), and $Pd(PPh_3)_4$ (114 mg, 98.7 mmol, 2.3 mmol %). The suspension was bubbled with N_2 via cannula for 20 min and then stirred at 110 °C for 14 h. The bright orange solid was isolated by filtration and successively washed with 25 mL each of water, 1 N HCl, and acetone. The material was purified by vacuum sublimation (P < 10^{-5} Torr) to afford 1.60 g (73%). DSC data (20 °C min^{-1}): peak temp 420 °C (ΔH = 246 J g^{-1}). HREIMS: calcd. for $C_{36}H_{22}S_2$ [M^+], 518.1163; found, 518.1155. Anal. Calcd for $C_{36}H_{22}S_2$: C, 83.36%; H, 4.28%; S, 12.36%. Found: C, 82.9%; H, 4.13%; S, 12.60%. Fluorescence spectrum (saturated toluene, right angle geometry, excitation at 400 nm): λ_{max} = 476 nm. Excitation spectrum (saturated toluene, monitoring fluorescence at 476 nm, λ_{max} (spectral response)): 359 (1.0), 416 (0.78).

2.B. Film Growth and Characterization. Thin films were grown by subliming **1** and **2** under vacuum from an alumina crucible in a Radak I furnace with feedback temperature control onto a resistively heated and water-cooled copper block. More details of the experimental setup have been reported previously.[23] Chamber pressure was typically 1×10^{-6} Torr and 4×10^{-7} Torr at the start and end of depositions, respectively. At these pressures, **1** and **2** began to sublime at 325 °C and 255 °C, respectively. The effect of substrate temperature on film growth was investigated from 25 °C to 275 °C for **1** and 25 °C to 200 °C for **2**. Film thickness was measured by a quartz crystal monitor. The growth rate was held at 0.02−0.03 Å/s for the first 3 layers (∼95 Å and ∼81 Å for **1** and **2**, respectively) and then increased to 0.1−0.2 Å/s to give a total thickness of 350 Å.

The structure and crystallinity of the thin films were characterized by wide-angle X-ray diffraction using a Philips X'Pert system with Cu Kα_1 (λ = 1.5406 Å) radiation. Standard $\theta-2\theta$ scans were acquired from 2° to 30°(2θ) at a step size of 0.015°(2θ) and a dwell time of 1 s per step. Powder XRD was also performed with the Philips X'Pert system with the same parameters from 2 to 35°(2θ). Grazing incidence X-ray diffraction (GIXD) was performed at the Stanford Synchrotron Radiation Lab (SSRL) using beamline 7-2 at an incident angle of 0.17° and an X-ray energy of 9.0 keV.

Thin-film morphology was examined using optical and atomic force microscopy (AFM). An Olympus (1000×) optical microscope with

(17) Meng, H.; Bao, Z.; Lovinger, A. J.; Wang, B.-C.; Mujsce, A. M. *J. Am. Chem. Soc.* **2001**, *123*, 9214−9215.
(18) Sirringhaus, H.; Kawase, T.; Friend, R. H.; Shimoda, T.; Inbasekaran, M.; Wu, W.; Woo, E. P. *Science* **2000**, *290*, 2123−2126.
(19) Sirringhaus, H.; Wilson, R. J.; Friend, R. H.; Inbasekaran, M.; Wu, W.; Woo, E. P.; Grell, M.; Bradley, D. D. C. *Appl. Phys. Lett.* **2000**, *77*, 406−408.
(20) Conjugation between anthracene and bithiophene is more effective through the 2-position of anthracene than at the 9-position; see: Würthner, F.; Vollmer, M. S.; Effenberger, F.; Emele, P.; Meyer, D. U.; Port, H.; Wolf, H. C. *J. Am. Chem. Soc.* **1995**, *117*, 8090−8099.
(21) Medne, R. S.; Livdane, A. D.; Neiland, O. Y. *J. Org. Chem. USSR (Engl. Transl.)* **1977**, *13*, 572−575.
(22) Wei, Y.; Yang, Y.; Yeh, J.-M. *Chem. Mater.* **1996**, *8*, 2659−2666.
(23) Pesavento, P. V.; Chesterfield, R. J.; Newman, C. R.; Frisbie, C. D. *J. Appl. Phys.* **2004**, *96*, 7312−7324.

Scheme 2. Synthesis of **1**

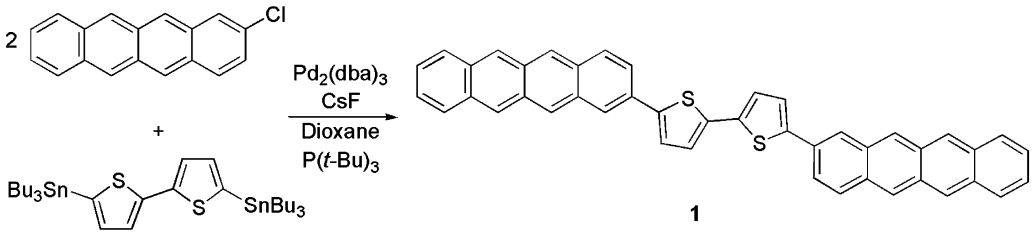

Scheme 3. Synthesis of **2**

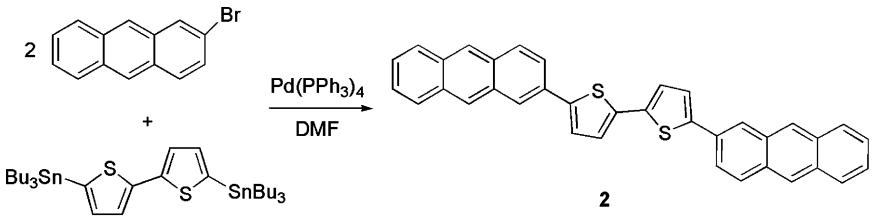

bright-field, dark-field, and differential interference contrast (DIC) modes was used to study grain size and film cracking. More detailed topographical data were obtained with a Digital Instruments Dimension 3100 AFM. Images were taken in air with Si cantilevers (MicroMasch) in tapping mode.

2.C. Substrate Preparation and Device Fabrication. Heavily doped p-type silicon wafers (Silicon Valley Microelectronics) with 3000 Å of thermally grown silicon dioxide served as substrates for device fabrication. The SiO_2 on the back of the wafer was removed with buffered oxide etch to facilitate electrical contact to the heavily doped silicon, which served as the gate. Ohmic contact was made to the silicon by depositing aluminum (100 Å) and gold (750 Å) followed by rapid thermal annealing at 450 °C. The substrates were cleaned with a cycle of sonication in acetone for 10 min followed by ashing in O_2 plasma for 2 min. Substrates prepared in this manner will be referred to as bare SiO_2. In addition, a thin layer of ~100 Å of 680 kg/mol poly(α-methyl styrene) was spun coat onto some SiO_2 substrates according to the patent published by 3M Company.[24,25] These substrates will be referred to as PS−SiO_2.

Thin films (350 Å) of **1** and **2** were deposited on bare SiO_2 and PS−SiO_2 substrates through stainless steel shadow masks. The patterned organic film deposition reduces device leakage and improves the accuracy of the four-probe measurement. Source, drain, and voltage sensing electrodes were deposited onto the films by thermal evaporation of 500 Å of Au through a silicon shadow mask. Gold (99.99%) was obtained from W. E. Mowrey & Co. The transistor channel had a width (W) of 2000 μm and a length (L) of 200 μm. Voltage sensing electrodes (~10 μm width) are located at ($^1/_3$)L and ($^2/_3$)L and penetrate the channel 125 μm. A schematic of the device structure and optical micrograph of a completed transistor are shown in Figure 1.

2.D. Electrical Characterization. Electrical characterization was performed in the dark using a Desert Cryogenics probe station with a base pressure of 5×10^{-7} Torr. Temperature was controlled via a Lakeshore L-331 controller between 80 and 325 K. After initial characterization at 295 K, the temperature was increased to 325 K and then decreased in 10 K increments to 85 K with an additional temperature data point taken at 80 K. Source and drain voltages were applied with a Keithley 236 and Keithley 237 source measure unit, respectively. Gate voltages were applied with a Keithley 6517A electrometer. Channel voltages were sensed with a pair of Keithley 6517A electrometers. Source and drain currents were independently monitored by the 236 and 237, respectively, to evaluate potential leaks in the devices. All four units shared a common ground and had an input impedance of 10^{14} Ω. All leads except the gate used triaxial cables with the electrometers run in guarded mode to minimize electrical noise and leakage currents.

Linear (μ_{lin}) and saturation (μ_{sat}) regime mobility were calculated based on standard metal-oxide-semiconductor field-effect transistor (MOSFET) equations. μ_{lin} was calculated using the transconductance (g_m) at a specific drain voltage. μ_{sat} was calculated from the slope of a $(I_D)^{1/2}$ versus gate voltage plot. Contact-corrected linear mobility (μ_{12}) was calculated as described in the TFT contact characterization section (3.F.). The turn-on voltage (V_0) was determined as the onset of exponential current increase from a logarithmic plot of drain current (log I_D) versus gate voltage (V_G). I_D-V_G sweeps were taken in 1.0 V gate steps from +50 V to −100 V back to +50 V. A typical sweep

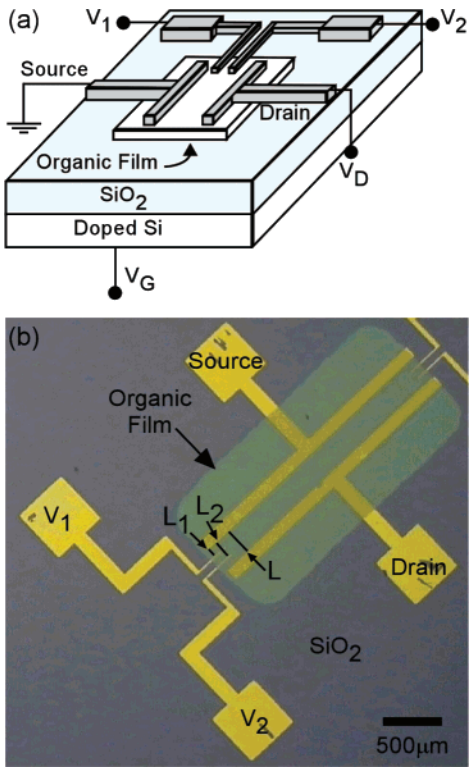

Figure 1. (a) Schematic of top-contact four-probe transistor geometry. (b) Optical micrograph of a completed transistor. The gold contacts are deposited on top of the organic film through a shadow mask.

(24) Kelley, T. W.; Boardman, L. D.; Dunbar, T. D.; Jones, T. D.; Muyres, D. V.; Pellerite, M. J.; Smith, T. P. Organic thin film transistor with polymeric interface. PCT Int. Appl. 03/041185 A2, May 15, 2003.
(25) Kelley, T. W.; Muyres, D. V.; Baude, P. F.; Smith, T. P.; Jones, T. D. *Mater. Res. Soc. Symp. Proc.* **2003**, *771*, 169−179.

Table 1. Summary of Thermal Analysis of **1**, **2**, and Pentacene, for Comparison

method	atmosphere	compound	mp (°C)	dec[a] (°C)
DSC/TGA[b]	N_2	**1**	533	535
TGA/DTA[c]	N_2	**1**	521	530
TGA/DTA	air	**1**		485
DSC/TGA	N_2	**2**	420	450
TGA/DTA	N_2	**2**	417	424
TGA/DTA	air	**2**	415	429
DSC/TGA	N_2	pentacene		339
TGA/DTA	N_2	pentacene		323
TGA/DTA	air	pentacene		319

[a] The spread in the decomposition values is due to the different scan rates (10 and 20 °C/min) employed in the two sets of TGA experiments. [b] Melting points are listed as the peak temperature of the mp endotherm in a DSC scan at 20 °C/min. The decomposition point is listed as the temperature at which 1% of the mass is lost as determined by a TGA experiment (20 °C/min) run at atmospheric pressure and under nitrogen. [c] Melting points are listed as the peak temperature of the mp endotherm in a DTA scan at 10 °C/min. The decomposition point is listed as the temperature at which 1% of the mass is lost as determined by a TGA experiment (10 °C/min) run at atmospheric pressure in either nitrogen or air.

took about 3 min for each drain voltage. I_D-V_D sweeps were taken in 1.0 V drain steps from 0 V to −60 V back to 0 V for all devices. Typical sweeps took 100 s for each gate voltage.

3. Results and Discussion

3.A. Synthesis. The final step in the synthesis of each of the acene−thiophene hybrids is a Stille cross-coupling[26] between an acenyl-halide and 5,5′-bis(tri-*n*-butylstannyl)-2,2′-bithiophene. The use of 2-chlorotetracene in a coupling reaction is noteworthy, since aryl chlorides are typically reluctant coupling partners. Nevertheless, using a recently published catalyst system[27] we have successfully used 2-chlorotetracene as an intermediate to new acene−thiophene oligomers. The yields reported above are for sublimed product and are over 70% for **2**. The somewhat lower yield (53%) of **1** was accompanied by a 17% recovery of 2-chlorotetracene starting material, which was readily isolated as a well-separated high vapor pressure fraction of the sublimation. Conditions for all of these reactions are unoptimized. We expect that related cross-coupling reactions of 2-chlorotetracene will yield a rich variety of new structures.

The acene−thiophene hybrids were characterized by elemental analysis, DSC, TGA, and DTA. Prominent base peaks for the molecular ions were observed in the mass spectra. Due to low solubility, characterization by solution phase techniques was not possible. The proposed connectivity is consistent with what is typically observed with Stille coupling reactions between aryl halides and stannyl thiophenes.

3.B. Thermal Analysis. Good thermal stability is important, since it is likely related to practical concerns such as ease of purification and device longevity. Table 1 lists the melting points (mp) and decomposition (dec) points for **1** and **2** and, for comparative purposes, pentacene. No char or discoloration of the hybrid materials is evident after thin-film deposition experiments. As determined experimentally by DSC, DTA, and TGA experiments, **1** has remarkable thermal stability for an organic material. Appreciable decomposition of **1** (under nitrogen) does not take place until the temperature exceeds 530 °C. A mp was observed just before decomposition at 521 °C by DTA and 533 °C by DSC. It is interesting to note that no mp was observed for **1** in air, and the decomposition temperature decreased to 485 °C. Compound **2** exhibited a stable mp in air and nitrogen at ∼417 °C followed by decomposition. The spread in the decomposition values is due to the different scan rates (10 and 20 °C/min) employed in the two sets of TGA experiments.

A purified pentacene sample began a gradual decomposition at ∼320 °C and showed no discernible mp in any experiment. The increased thermal stability of hybrid materials should be a feature that positively affects device stability and lifetime.

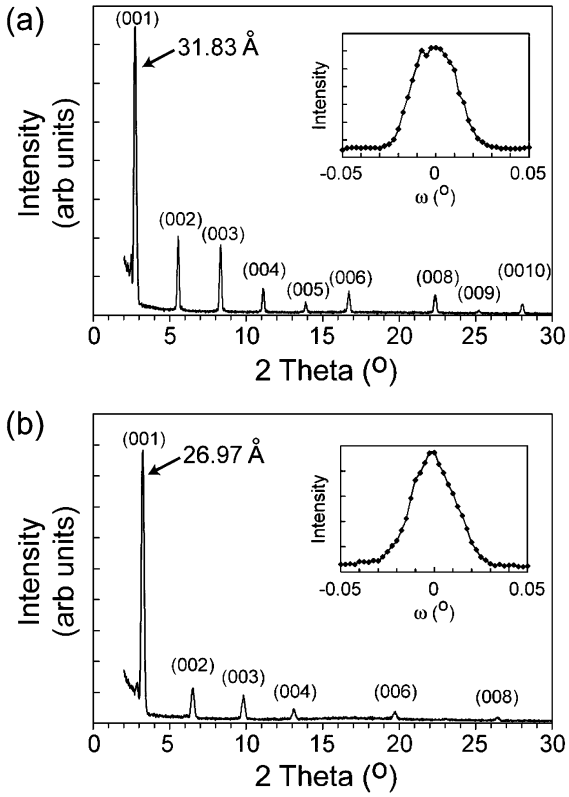

Figure 2. (a) Thin-film X-ray diffraction pattern for a 500 Å film of **1** on PS−SiO_2 grown at T_s = 260 °C. The inset shows a rocking curve across the (001) reflection for this film with a fwhm of 0.031°. (b) Thin-film X-ray diffraction pattern for a 350 Å film of **2** on bare SiO_2 grown at T_s = 100 °C. The inset shows a rocking curve across the (001) reflection for this film with a fwhm of 0.028°.

3.C. Thin-Film Morphology. The thin-film morphology of **1** was characterized for substrate growth temperatures of 25−275 °C. Above 260 °C, discontinuous films were obtained due to the significant decrease in the molecules' sticking coefficient at this temperature. Grain size increased with increasing substrate temperature from <100 nm at room temperature to ∼3 μm at 260 °C on PS−SiO_2. Film cracking during cooling became an issue at higher substrate temperatures and for larger grain sizes. The effect of cracking was mitigated by postdeposition cooling at ∼5 °C/min.

Films deposited on bare SiO_2 and PS−SiO_2 were highly crystalline as shown in Figure 2a. All films exhibited (001), (002), (003) reflections, and crystallinity increased as T_s increased (more higher order peaks were seen). Increasing film thickness up to 750 Å permitted observation of peaks up to

(26) Farina, V.; Krishnamurthy, V.; Scott, W. J. *Org. React. (New York)* **1997**, *50*, 1−652.
(27) Littke, A. F.; Schwarz, L.; Fu, G. C. *J. Am. Chem. Soc.* **2002**, *124*, 6343−6348.

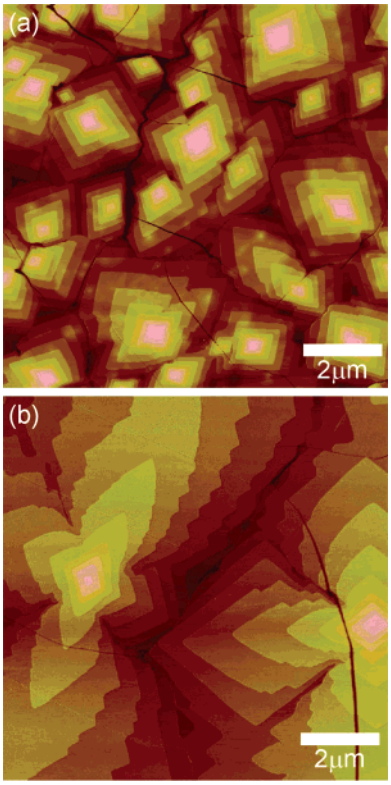

Figure 3. (a) AFM topographical image of grains of **1** on PS−SiO_2 grown at $T_s = 260$ °C. (b) AFM topographical image of grains of **2** on bare SiO_2 grown at $T_s = 100$ °C.

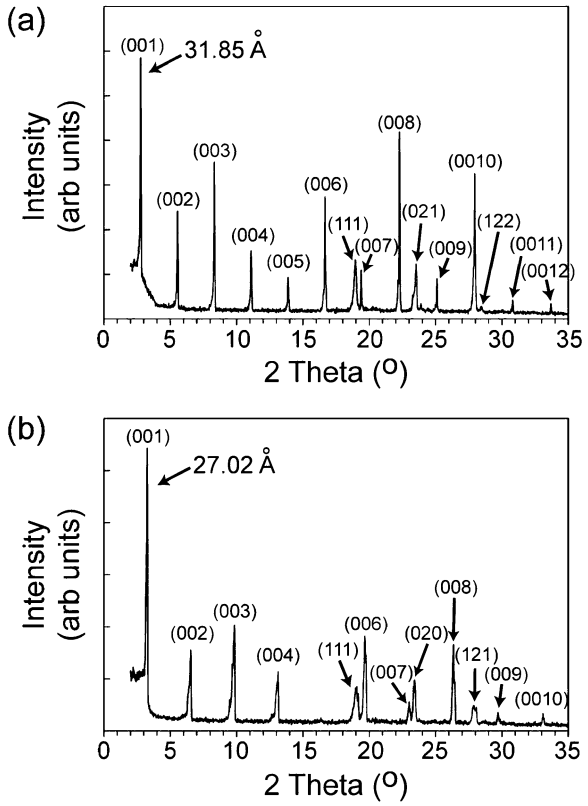

Figure 4. (a) Powder XRD of **1**. The peaks have been indexed based on the thin-film XRD and GIXD data. (b) Powder XRD of **2**.

(0012). Films of **1** packed identically on bare SiO_2 and PS−SiO_2 with the primary peak at $2\theta = 2.77°$, corresponding to a *d* spacing of 31.83 Å. X-ray rocking curves across the (001) reflections from films of **1** gave widths of 0.030°−0.035°. The rocking curve for a film of **1** is shown in the inset of Figure 2a, and the narrow width is indicative of a high degree of in-plane ordering. These values compare well with highly ordered films of other organic semiconductors.[28−30] It is interesting to note that the (007) peak was not observed for any films grown. A systematic absence of this peak is not consistent with the symmetry of the thin-film unit cell discussed below, and the absence of this peak is likely due to structure factor considerations.

Figure 3a shows an AFM topographical image of terraced grains with a stepheight of 32 ± 1 Å, corresponding to the *d* spacing of 31.83 Å observed in the XRD pattern. Due to growth at elevated temperatures, cracks within the film are evident. In addition, it is possible the PS and **1** could intermix at the elevated substrate temperatures, but no structural (via XRD) or electrical behavior was observed that indicated mixing of PS and **1**. The glass transition temperature (T_g) for bulk PS film is ∼100 °C.[31] However, thin films of PS have depressed T_g values,[32] and it is expected that the ∼100 Å film employed for this work has a T_g ∼50 °C, implying nearly all growths were performed above T_g.

The thin-film morphology of **2** was investigated in the same manner as **1** for a range of substrate temperatures from 25 to 200 °C. Film continuity became an issue above 175 °C. Faceted, arrowhead-like grains were observed for growths on bare SiO_2. Growth on PS−SiO_2 was less consistent, but the observed morphology was similar. It is interesting to note the difference in preferred substrate for growth of the two compounds. A similar situation is seen for tetracene and pentacene growth on bare SiO_2. Tetracene films have loosely connected grains, while pentacene forms dense, highly crystalline films in which there is good grain-to-grain contact.[13] It is clear that the detailed interactions involved in organic semiconductor thin-film growth are not well understood.

Films on bare SiO_2 and PS−SiO_2 were highly crystalline, similar to **1**, as seen in Figure 2b. The primary peak at $2\theta = 3.27°$ corresponds to a *d* spacing of 26.97 Å. The large, terraced grains observed with AFM have a stepheight of 27 ± 1 Å, in agreement with the *d* spacing from XRD. Films of both **1** and **2** exhibited a high degree of in-plane ordering. X-ray rocking curves across the (001) reflections of the films of **2** gave widths of 0.028°−0.032°. The rocking curve for a film of **2** is shown in the inset of Figure 2b.

3.D. Powder and Thin-Film Grazing Incidence X-ray Diffraction. Figure 4 shows the powder XRD patterns for **1** and **2**. Both spectra exhibit many of the same peaks (and *d* spacing) seen in the corresponding thin-film XRD spectra. Therefore, the thin-film packs in a single-crystal like (bulk) manner. For powders of **1**, additional peaks were observed at 19.0° (111), 23.5° (021), and 28.0° (122) with additional peaks at 19.0° (111), 23.4° (020), and 27.9° (121) for powders of **2**. Because the comparison of the thin-film XRD and powder

(28) Karl, N. *Synth. Met.* **2003**, *133*−*134*, 649−657.
(29) Durr, A. C.; Schreiber, F.; Munch, M.; Karl, N.; Krause, B.; Kruppa, V.; Dosch, H. *Appl. Phys. Lett.* **2002**, *81*, 2276−2278.
(30) Karl, N.; Kraft, K. H.; Marktanner, J.; Munch, M.; Schatz, F.; Stehle, R.; Uhde, H. M. *J. Vac. Sci. Technol., A* **1999**, *17*, 2318−2328.
(31) Bliznyuk, V. N.; Assender, H. E.; Briggs, G. A. D. *Macromolecules* **2002**, *35*, 6613−6622.
(32) Ellison, C. J.; Torkelson, J. M. *Nat. Mater.* **2003**, *2*, 695−700.

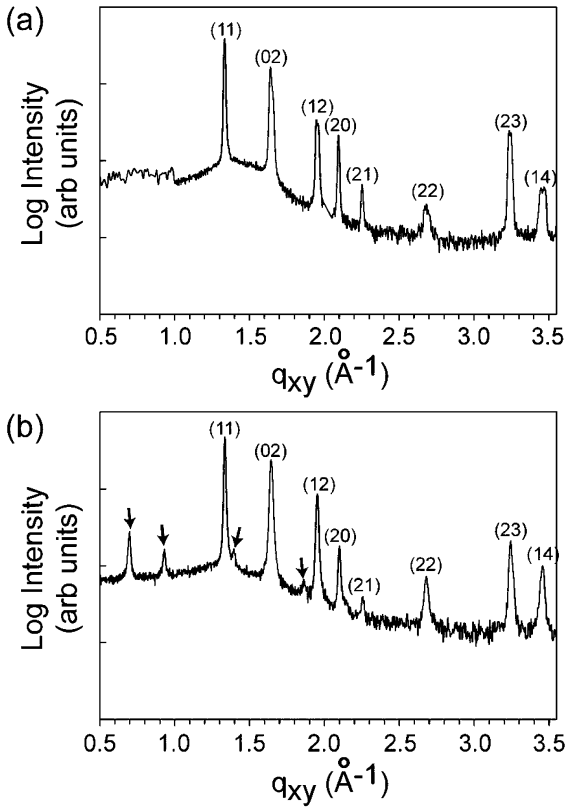

Figure 5. (a) GIXD pattern for a 350 Å film of **1** on PS−SiO_2. (b) GIXD pattern for a 350 Å film of **2** on bare SiO_2.

patterns revealed the thin-film structure is the bulk structure, the peaks other than (00*l*) were indexed based on the thin-film unit cell parameters obtained from the GIXD data discussed below. The powder pattern is consistent with the GIXD data, and the strongest peaks observed in the GIXD spectra are seen at the expected 2θ values in the powder pattern.

GIXD was performed to determine the thin-film unit cell parameters of **1** and **2**. Figure 5 shows the GIXD patterns (intensity vs q_{xy}) for **1** and **2**. From these data, the in-plane lattice parameters (*a*,*b*) and the angle between them (γ) can be determined (see Supporting Information for more details). Films of **1** exhibited two slightly different phases as evidenced by the doublets of several peaks (see Supporting Information Figure S2) in the diffraction patterns. Clear determination of the two phases was not successful, and more data will be needed to resolve them. Using the first peak of each pair of doublets, the peaks are indexed to a rectangular in-plane unit cell with dimensions $a = 5.993$ Å, $b = 7.659$ Å, and $\gamma = 90.0°$. For **2**, a similar in-plane unit cell was found with $a = 5.980$ Å, $b = 7.644$ Å, and $\gamma = 90.0°$. Not surprisingly, both molecules have nearly the same in-plane unit cell geometry and area. There are two molecules per unit cell similar to the pentacene structure.[33,34] The calculated densities of **1** and **2** are 1.41 g/cm^3 and 1.39 g/cm^3, respectively, from the given unit cells. These density values are comparable to other common organic semiconductors such as pentacene[33,34] (1.36 g/cm^3) and sexithiophene[35] (1.55 g/cm^3). Several of the peaks seen in the spectrum of **2** (denoted by arrows in Figure 5b) are not consistent with this lattice parameter assignment and appear to be a second phase. The peaks at $q_{xy} = 0.698$, 0.932, 1.396, and 1.864 Å^{-1} (denoted by arrows) are weaker in intensity and correspond to *d* spacings of 9.00, 6.74, 4.50, and 3.37 Å, which are the values for the (003), (004), (006), and (008) reflections from thin-film XRD. These peaks suggest that some fraction of the molecules is lying down (i.e., long axis of the molecule parallel to the surface). For thicker films (∼750 Å) of **2**, the (110) peak was observed in thin-film XRD spectra (See Supporting Information Figure S1), which supports this hypothesis. Some fraction of the molecules lying down is likely to have a detrimental effect on the electronic transport properties of films of **2**, since the preferred transport direction occurs within the *ab* plane.[2]

Table 2. Summary of Thin-Film Lattice Parameters for **1** and **2**

	1	2
a (Å)	5.993 ± 0.005	5.980 ± 0.005
b (Å)	7.659 ± 0.005	7.644 ± 0.005
c (Å)	31.98 ± 0.01	27.22 ± 0.01
α (deg)	93.0 ± 0.4	94.0 ± 0.4
β (deg)	85.5 ± 0.4	84.5 ± 0.4
γ (deg)	90.0 ± 0.1	90.0 ± 0.1
area (Å^2)	45.90	45.71

With a full set of q_{xy} and q_z data, the complete thin-film unit cell can be determined (See Supporting Information). Both films have triclinic cells, and the lattice parameters are summarized in Table 2. The d_{001} spacing calculated from these unit cells was 31.83 Å for **1** and 27.03 Å for **2**, which agrees well with the values from wide-angle XRD of 31.83 and 26.97 Å for films of **1** and **2**, respectively.

3.E. TFT Characterization. TFTs were characterized in a top contact geometry using Au contacts as shown in Figure 1. Typical I_D-V_G and I_D-V_D curves for **1** are shown in Figure 6. On/off current ratios of $>10^8$ were observed with negligible hysteresis in a vacuum. Contact-corrected p-channel linear mobility of 0.5 cm^2/Vs (0.42 cm^2/Vs uncorrected) was observed for **1** on PS−SiO_2 when $T_s = 175-215$ °C. Contact-corrected linear mobility of 0.18 cm^2/Vs (0.16 cm^2/Vs uncorrected) was observed on bare SiO_2 substrates when $T_s = 175-225$ °C. Working TFTs were possible at all substrate temperatures studied, and mobility generally increased with increasing T_s up to a plateau and then decreased again at the highest temperatures as film continuity suffered. Similar trends have been observed with compounds based on anthracene oligomers.[36,37] The contact-corrected linear mobility (μ_{12}) was consistent from device to device and had negligible drain voltage dependence.

Typical I_D-V_G and I_D-V_D curves for **2** are shown in Figure 7. On/off current ratios of $>10^8$ were observed. Contact-corrected p-channel linear mobility of 0.12 cm^2/Vs (0.095 cm^2/Vs uncorrected) was observed for **2** on bare and PS-treated SiO_2 when $T_s = 100-125$ °C. The temperature range over which high-mobility TFTs could be obtained was smaller with **2** than **1**. It is not unexpected that films of **1** have higher mobility than films of **2**. Mobility increases in the regular acene series of

(33) Holmes, D.; Kumaraswamy, S.; Matzger, A. J.; Vollhardt, K. P. C. *Chem.—Eur. J.* **1999**, *5*, 3399−3412.
(34) Mattheus, C. C.; Dros, A. B.; Baas, J.; Meetsma, A.; Boer, J. L. d. B.; Palstra, T. T. M. *Acta Crystallogr., Sect. C* **2001**, *C57*, 939−941.
(35) Horowitz, G.; Bachet, B.; Yassar, A.; Lang, P.; Demanze, F.; Fave, J.-L.; Garnier, F. *Chem. Mater.* **1995**, *7*, 1337−1341.
(36) Ito, K.; Suzuki, T.; Sakamoto, Y.; Kubota, D.; Inoue, Y.; Sato, F.; Tokito, S. *Angew. Chem., Int. Ed.* **2003**, *42*, 1159−1162.
(37) Inoue, Y.; Tokito, S.; Ito, K.; Suzuki, T. *J. Appl. Phys.* **2004**, *95*, 5795−5799.

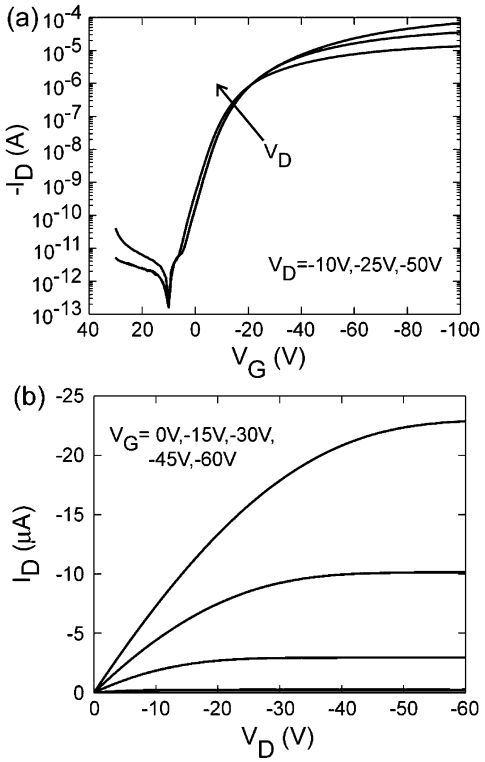

Figure 6. (a) I_D-V_G characteristics for $V_D = -10$, -25, and -50 V for a typical TFT of **1** on PS$-$SiO$_2$ at 295 K. The data took 9 min to acquire. Hysteresis was <15% between forward and reverse traces. (b) I_D-V_D curves for same device at 295 K. The data took 7.5 min to acquire. Hysteresis was less <1.5% between forward and reverse traces.

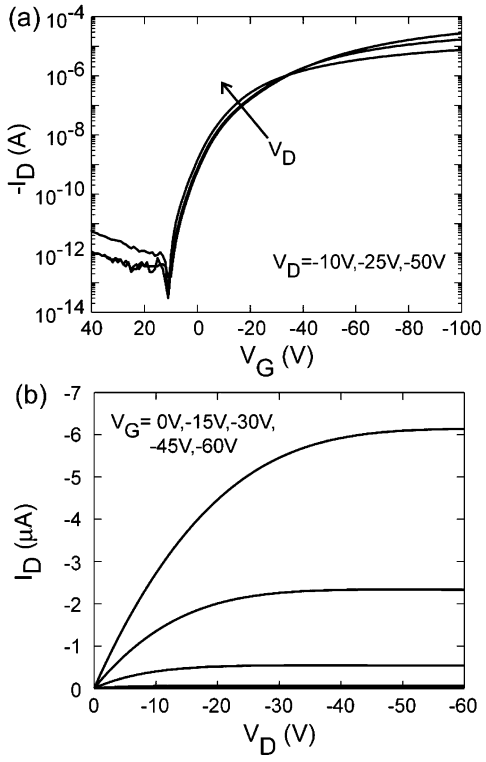

Figure 7. (a) I_D-V_G characteristics for $V_D = -10$, -25, and -50 V for a typical TFT of **2** on SiO$_2$ at 295 K. Hysteresis was <2% between forward and reverse traces. (b) I_D-V_D curves for same device at 295 K. Hysteresis was <3% between forward and reverse traces.

anthracene, tetracene, and pentacene with increasing conjugation length.[38]

3.F. Contact Effects. The Au contacts to thin films of **1** and **2** were characterized using the four-probe method that has been applied to organic semiconductors[23,38−44] and a-Si:H.[45−47] Two voltage sensing electrodes (V_1 and V_2) are equally spaced within the channel. These electrodes sense the potential in the channel and can be used to extract the contact resistance of the source and drain electrodes independently. The four-probe method is only valid in the linear regime of device operation where $(V_G - V_T) \gg V_D$ and the gradual channel approximation holds. Based on a linear extrapolation of the voltage between the sense probes, the source (ΔV_S) and drain (ΔV_D) contact voltage drops are given by

$$\Delta V_S = \frac{L_2 V_1 - L_1 V_2}{L_2 - L_1} - V_S \qquad (1)$$

$$\Delta V_D = V_D - \frac{L(V_2 - V_1) + L_2 V_1 - L_1 V_2}{L_2 - L_1} \qquad (2)$$

where V_S, V_D, V_1, and V_2 are the voltages at the source electrode, drain electrode, first sense electrode, and second sense electrode, respectively, and L, L_1, and L_2 are the distances measured from source to drain, source to the first sense electrode, and source to the second sense electrode, respectively. The corresponding contact resistances can be calculated by dividing each contact voltage drop by I_D.

In addition to calculating contact resistance, a contact-corrected linear mobility (μ_{12}) can be extracted by casting the standard linear regime transistor equation in terms of channel probe parameters

$$\frac{I_D}{V_{12}} = \frac{W}{L_2 - L_1}\mu_{12} C_{ox}(V_{G12} - V_{T12}) \qquad (3)$$

$$g_{m12} = \frac{d}{V_{G12}}\left(\frac{I_D}{V_{12}}\right) = \frac{W}{L_2 - L_1}\mu_{12} C_{ox} \qquad (4)$$

where I_D is the drain current, $V_{12} = V_2 - V_1$, C_{ox} is the capacitance of the oxide per unit area, $V_{G12} = V_G - (V_1 + V_2)/2$ is the effective gate field in the middle of the channel, and V_{T12} is the contact-corrected threshold voltage. The contact-corrected linear mobility can be calculated using eq 4.[48] This method was used to calculate all linear mobility values given in this paper.

Figure 8 shows the resistance of the film, source contact, and drain contact as a function of gate voltage for $V_D = -10$ V for

(38) De Boer, R. W. I.; Gershenson, M. E.; Morpurgo, A. F.; Podzorov, V. *Phys. Status Solidi A* **2004**, *201*, 1302−1331.
(39) Merlo, J. A.; Frisbie, C. D. *J. Polym. Sci., Part B: Polym. Phys.* **2003**, *41*, 2674−2680.
(40) Podzorov, V.; Pudalov, V. M.; Gershenson, M. E. *Appl. Phys. Lett.* **2003**, *82*, 1739−1741.
(41) Takeya, J.; Goldmann, C.; Haas, S.; Pernstich, K. P.; Ketterer, B.; Batlogg, B. *J. Appl. Phys.* **2003**, *94*, 5800−5804.
(42) Goldmann, C.; Haas, S.; Krellner, C.; Pernstich, K. P.; Gundlach, D. J.; Batlogg, B. *J. Appl. Phys.* **2004**, *96*, 2080−2086.
(43) Yagi, I.; Tsukagoshi, K.; Aoyagi, Y. *Appl. Phys. Lett.* **2004**, *84*, 813−815.
(44) Chesterfield, R. J.; McKeen, J. C.; Newman, C. R.; Frisbie, C. D.; Ewbank, P. C.; Mann, K. R.; Miller, L. L. *J. Appl. Phys.* **2004**, *95*, 6396−6405.
(45) Hattori, R.; Kanicki, J. *Jpn. J. Appl. Phys., Part 2* **2003**, *42*, 907−909.
(46) Chiang, C.-S.; Chen, C.-Y.; Kanicki, J. *IEEE Electron Device Lett.* **1998**, *19*, 382−384.
(47) Liu, S.-D.; Shih, A.; Chen, S.-D.; Lee, S.-C. *J. Vac. Sci. Technol., B* **2003**, *21*, 677−682.
(48) Chen, C.-Y.; Kanicki, J. *IEEE Electron Device Lett.* **1997**, *18*, 340−342.

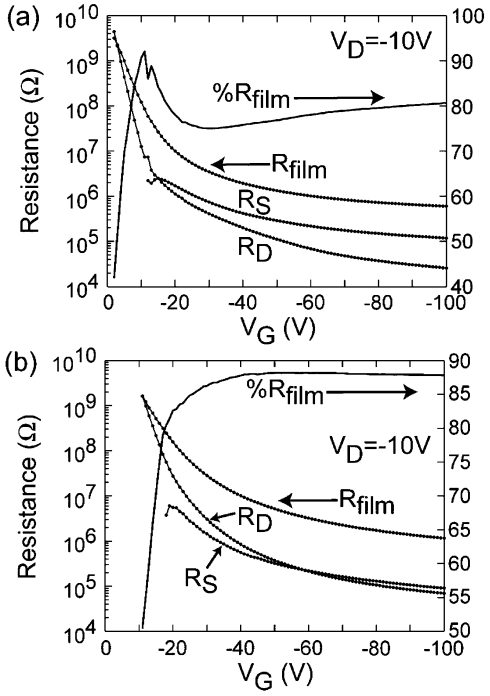

Figure 8. (a) Plot of film resistance, source, and drain contact resistance on the left axis as a function of gate voltage for a film of **1**. The right axis shows the film resistance (%R_{film}) as a percentage of the total device resistance. The linear extrapolation used to generate the contact resistance is only valid for $(V_G - V_T) \gg V_D$. (b) The corresponding plot for a film of **2**.

typical films of **1** and **2**. The gate voltage modulates all three resistances, which tend to level off at high gate voltage. The percentage of the resistance due to the film is given on the right axis of the same plot. For both compounds the majority of device resistance was due to the film and not the contacts as can be seen from the percentage of film resistance. The contact correction to the linear mobility based on the transconductance was typically 15−20% for **1** and 5−15% for **2**. Using eqs 1 and 2 to calculate voltage drops at the contacts and dividing by the corresponding drain current, room-temperature values for the combined specific contact resistance (at high gate voltage) for Au top contacts on films of **1** and **2** were 2×10^4 Ω cm and 3×10^4 Ω cm, respectively.

The four-probe geometry can also be used to measure the activation energy of the contacts by varying the temperature. For Au contacts to films of **1**, the activation energy of the combined contact resistance (source and drain) was 25 meV. This value is nearly the same as the activation energy for the film (22 meV) as will be discussed in the temperature dependence section. The contribution of the contact resistance to overall resistance stays constant at ∼19% from 80 to 295 K. The Au contacts to films of **2** exhibited an activation energy of 36 meV. The contacts have somewhat higher activation energy than the film (28 meV) and become a greater part of the overall device resistance as temperature is decreased. For TFTs of **2**, the contacts made up ∼10% of total resistance at room temperature and increased to ∼35% of total resistance at 80 K. The four-probe method allows the true activation energy of the film to be measured without impact from the activation energy of the contacts. A traditional transistor geometry yields an activation energy that is a convolution of film and contacts.

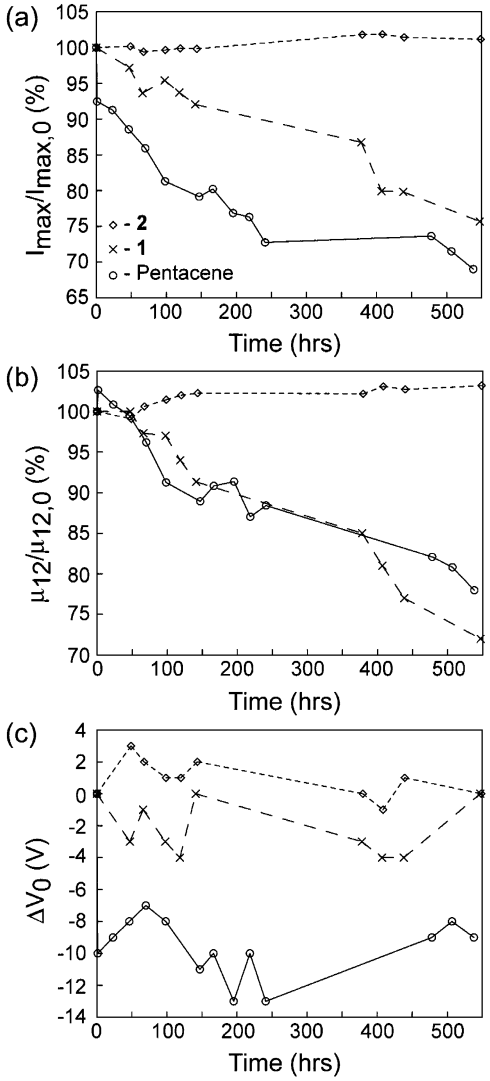

Figure 9. (a) Plot of percentage change in current at $V_D = -10$ V, $V_G = -100$ V versus time in air for each material. The lines serve as a guide to the eye in each figure. (b) Plot of percentage change in contact-corrected mobility (μ_{12}) versus time in air for each material. (c) Shift in V_0 as a function of time in air for each material. Note for pentacene there is a shift of −10 V in the first 2 h.

3.G. Air Stability. The long-term stability (over a three week period) of films of **1** and **2** stored in air was measured and compared to the benchmark organic semiconductor, pentacene. Films of pentacene were prepared in an analogous manner to **1** and **2** (350 Å on PS−SiO_2 deposited at $T_s = 25$ °C). $I_D - V_G$ traces at $V_D = -10$, −25, and −50 V were measured in air and darkness with storage in ambient conditions (room temperature in the dark) between measurements. The films had the following initial properties: pentacene ($\mu_{12} = 0.95$ cm^2/Vs, on/off current ratio 10^9), **1** ($\mu_{12} = 0.32$ cm^2/Vs, on/off current ratio 10^8), and **2** ($\mu_{12} = 0.11$ cm^2/Vs, on/off current ratio 10^7). The initial properties were taken as time equal to zero.

The change in maximum current at a given drain and gate voltage ($V_D = -10$ V, $V_G = -100$ V), change in μ_{12}, and turn-on voltage shift (ΔV_0) were used to qualify the device stability. Figure 9a−c show the evolution of these parameters as a function of time stored in air. To compare across materials, the current and contact-corrected mobility were normalized to the time equal zero value ($I_{max,0}$, $\mu_{12,0}$) and turn-on voltage shifts

are relative to the time equal zero value ($\Delta V_0 = V_0 - V_{0,0}$). Changes in transistor performance (i.e., instabilities) are most directly observed as a change in current at a given set of gate and drain voltages. However, changes in current over time can be due to several factors such as mobility changes, V_0 shifts, or changing contact resistance. Figure 9a shows the change in current for the three materials as a function of time in air. It is clear **1** and **2** are more air stable than pentacene. In fact, **2** exhibited no degradation of current over ~550 h, while the pentacene transistor lost 31% of the original current and **1** lost 24%. A previous study of pentacene FETs over 9 months[49] showed significant current degradation, while another group reported a nearly identical 30% drop in mobility over a 500 h period.[50] Figure 9b,c detail the changes in mobility and V_0 for the same transistors. Transistors of **2** were the most air stable and had only a slight variation in V_0 (3 V) and mobility (2%). For transistors of **1**, the loss in maximum current was mirrored by the same decrease in mobility with a variation of 4 V in V_0 values. Therefore, it appears the current degradation is solely due to a decrease in the mobility of the film. Pentacene exhibits a trend not seen in the other two compounds. The drop in contact-corrected mobility is consistently less (~10−15%) than the drop in maximum current. This phenomenon can be explained by a negative shift in V_0, which causes the maximum current to decrease due to the transistor not reaching an equivalent free carrier density. Within the first 12 h, the pentacene transistor has a large V_0 shift of −10 V, but the mobility is unaffected. After this point, the reduction in current is mirrored by a decreasing mobility, but an offset still remains from the V_0 shift. From the data, it appears **2** is truly air stable over the time period studied and **1** is more stable than pentacene but still subject to electrical degradation.

3.H. Temperature and Gate Voltage Dependence of the Mobility. Organic semiconductors typically show activated transport over a wide range of temperatures.[44,51−53] Figure 10a shows the evolution of the I_D-V_G traces for a TFT based on **1** as a function of temperature. It is clear that transport is activated from (1) the decrease in drain current as temperature is decreased, (2) the negative shift in the turn-on voltage (V_0) as temperature is decreased, and (3) the decrease in sharpness of the device turn-on (sharpness is inversely proportional to the sub-threshold swing = $dV_G/d(\log I_D)$) with reduced temperature. The evolution of I_D-V_G traces for films based on **2** is analogous. The V_0 shift (an average value of 5 TFTs for each compound) was 11 and 5.3 V, respectively, for TFTs based on **1** and **2**. The turn-on voltage is the point conduction is initiated at each temperature, and a rough calculation of the deep traps in the films can be made using $\Delta p = C_{ox}(V_{0,295K} - V_0)/e$. The number of deep donor-like states is estimated to be 7.8×10^{11} cm^{-2} (1 per 560 molecules if all traps are in one layer) and 3.8×10^{11} cm^{-2} (1 per 1150 molecules) for **1** and **2**, respectively. Figure 10b shows the mobility of films of **1** and **2** as a function of temperature on both substrates. The mobility decreases with temperature, which is indicative of activated transport.

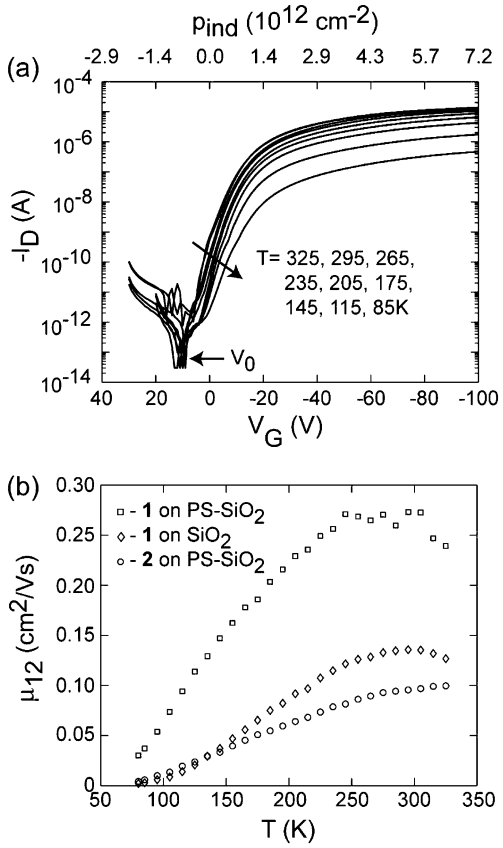

Figure 10. (a) Evolution of I_D-V_G traces as a function of temperature for a TFT based on **1** ($V_D = -10$ V, oxide thickness = 3000 Å). The traces span 325 K to 85 K in increments of 30 K. A small shift in the turn-on voltage (V_0) is observed. (b) Contact-corrected linear mobility versus temperature for films of **1** and **2** on bare SiO_2 and PS−SiO_2 at the highest gate voltages studied. The data for **2** on bare SiO_2 have been omitted for clarity, since they are nearly identical to the data for PS−SiO_2.

Two common models for thermally activated transport are multiple trapping and release (MTR)[52] and variable range hopping (VRH).[54] MTR assumes most of the injected carriers are trapped in a distribution of states in the band gap and are thermally activated to mobile states. MTR predicts decreasing activation energy with increasing gate voltage as the Fermi level of the material moves through the distribution of states and closer to the valence band edge. MTR proposes that the effective mobility (μ_{eff}) is the free carrier mobility (μ_0) multiplied by the ratio of free holes (N_{free}) to total induced holes (N_{tot}).

$$\mu_{eff}(V_G,T) = \mu_0 \frac{N_{free}}{N_{tot}} \tag{5}$$

The VRH model of Vissenberg et al.[54] proposes that transport occurs via hopping in an exponential distribution of localized states. Mobility is thermally activated and follows a simple Arrhenius relationship. This prediction is different than Mott VRH where $\mu \approx \exp[-(T_0/T)^{1/3}]$ for two-dimensional hopping.[55] Mott VRH assumes hopping through a constant density of states, which leads to the different temperature dependence. The Vissenberg model predicts gate-voltage dependent mobility and

(49) Pannemann, C.; Diekmann, T.; Hilleringmann, U. *J. Mater. Res.* **2004**, *19*, 1999−2002.
(50) Qui, Y.; Hu, Y.; Dong, G.; Wang, L.; Xie, J.; Ma, Y. *Appl. Phys. Lett.* **2003**, *83*, 1644−1646.
(51) Sirringhaus, H.; Tessler, N.; Friend, R. H. *Science* **1998**, *280*, 1741−1744.
(52) Horowitz, G.; Hajlaoui, R.; Delannoy, P. *J. Phys. III* **1995**, *5*, 355−371.
(53) Knipp, D.; Street, R. A.; Volkel, A. R. *Appl. Phys. Lett.* **2003**, *82*, 3907−3909.
(54) Vissenberg, M. C. J. M.; Matters, M. *Phys. Rev. B: Condens. Matter* **1998**, *57*, 12964−12967.
(55) Mott, N. F.; Davis, E. A. *Electronic Processes in Non-Crystalline Materials*, 2nd ed.; Clarendon Press: Oxford, 1979.

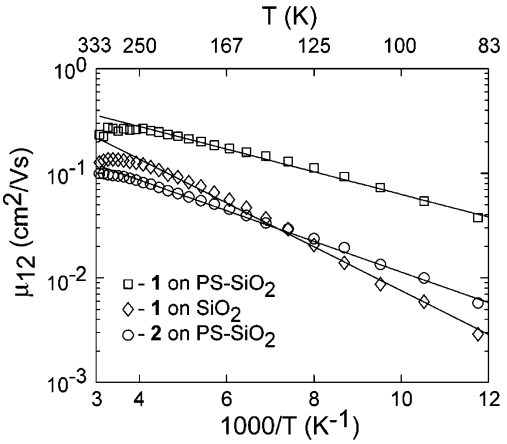

Figure 11. Contact-corrected linear mobility versus inverse temperature for films of **1** and **2** on bare SiO_2 and PS−SiO_2. The lines indicate fits to a simple Arrhenius expression to get the activation energy.

activation energy similar to MTR. As the gate voltage is increased, carriers fill the lower energy states. Additional carriers begin to fill higher energy states, which require lower activation energy to hop to the next site. Consequently, the activation energy decreases, and the mobility increases with increasing gate voltage.

Hopping in an exponential distribution of states can also be described in terms of an effective transport energy level.[56,57] Carriers are activated from the Fermi level to the transport energy. Hopping transport described in this fashion closely resembles the formalism of MTR with a single trap level. Therefore, it is difficult to distinguish between MTR and VRH in a distribution of trap states based on mobility versus temperature data. Due to the high degree of ordering indicated by the XRD results, MTR seems like the more plausible model for thin films of **1** and **2**. Transport in organic thin films has been described previously in terms of VRH[58] and MTR.[44,53,59,60]

Figure 11 shows the Arrhenius plot of mobility versus inverse temperature for the data shown in Figure 10b. The lines represent fits to the data from 85 to 265 K. Films of **1** have an activation energy of 22 meV (PS−SiO_2) and 38 meV (SiO_2) while films of **2** exhibit an activation energy of 28 meV (PS−SiO_2) and 27 meV (SiO_2). Since the activation energies for **1** and **2** are similar, it is possible that both molecules have the same dominant trap or traps. The greater activation energy of **1** on bare SiO_2 compared to PS−SiO_2 may help to explain the lower mobility of films of **1** on bare SiO_2. The larger activation energy is indicative of more and/or deeper traps, which leads to a decreased mobility in the framework of the MTR model. All films show a gate-voltage-dependent activation energy with about a factor of 2 higher activation energy at low gate voltages than the values quoted (at high gate voltage). To gain further understanding of the traps in the films, we modeled the hole trap (donor-like) states as a double exponential distribution as described below.

The MTR model assumes a specific energy exists that defines the boundary between localized states and mobile states. Similar to Salleo et al.,[61] we define the mobility edge as $E = 0$ at the top of the mobile states. The density of states ($D(E)$) in the mobile states is taken as $D(E) \approx E$ as in a-Si:H.[62] The localized donor-like states are taken to be a double exponential distribution

$$D_{\mathrm{trap}}(E) = \frac{N_{\mathrm{td}}}{E_{\mathrm{td}}}\exp\left(-\frac{E}{E_{\mathrm{td}}}\right) + \frac{N_{\mathrm{dd}}}{E_{\mathrm{dd}}}\exp\left(-\frac{E}{E_{\mathrm{dd}}}\right) \qquad (6)$$

where N_{td} is the total concentration (in cm^{-3}) of shallow tail states, E_{td} is the width (in eV) of the shallow tail states, N_{dd} is the total concentration (in cm^{-3}) of deep tail states, and E_{dd} is the width (in eV) of the deep tail states. Previous work has assumed a single-exponential distribution for a conducting polymer[61] and a double exponential distribution to model the density of states of vapor deposited derivatives of sexithiophene[52] and a-Si:H.[62−64] Disordered polymer systems are commonly modeled as a Gaussian distribution of states.[65−67]

To determine the trap state concentrations and widths in eq 6, the experimental mobility versus gate voltage and temperature data were fit iteratively using eq 5. The total induced charge in the organic semiconductor is given by (assuming a fixed thickness of the conducting channel)

$$N_{\mathrm{tot}}(V_{\mathrm{G}},T) = \frac{C_{\mathrm{ox}}|V_{\mathrm{G}} - V_0|}{h} = \int_{-\infty}^{+\infty} D(E)\, f(E_{\mathrm{F}},E)\, \mathrm{d}E \quad (7)$$

where C_{ox} is the capacitance of the oxide per unit area, V_0 is the turn-on voltage, h is the thickness of the channel (taken to be one monolayer; 3.18 nm for **1** and 2.70 nm for **2**), $D(E)$ is the density of states in the organic semiconductor, $f(E_{\mathrm{F}},E)$ is the Fermi−Dirac distribution, and E_{F} is the Fermi level. By making guesses for N_{td}, E_{td}, N_{dd}, and E_{dd}, eq 7 can be solved numerically for the position of the Fermi level $E_{\mathrm{F}}(V_{\mathrm{G}} - V_0, T)$. Once the evolution of the Fermi level is known, the number of mobile carriers can be calculated using

$$N_{\mathrm{free}}(V_{\mathrm{G}},T) = \int_{-\infty}^{0} D(E)\, f(E_{\mathrm{F}},E)\, \mathrm{d}E \qquad (8)$$

Equation 5 can then be used (with a guess of μ_0) to calculate $\mu(V_{\mathrm{G}} - V_0, T)$. A set of values for N_{td}, E_{td}, N_{dd}, E_{dd}, and μ_0 is found iteratively by minimizing the least squares error between μ(predicted) and μ(measured). Figure 12a shows a plot of contact corrected mobility versus inverse temperature for four different values of $V_{\mathrm{G}} - V_0$ and the corresponding fits using the method described above. The model fits deviate from the data above 295 K where the mobility has a weaker temperature dependence, but the double exponential distribution represents the data better than the simple Arrhenius fit in Figure 11. Attempts to fit the mobility data with a single-exponential distribution were unsuccessful. The values used for the fit parameters are $N_{\mathrm{td}} = 2 \times 10^{20}$ cm^{-3}, $E_{\mathrm{td}} = 12.5$ meV, $N_{\mathrm{dd}} =$

(56) Baranovskii, S. D.; Faber, T.; Hensel, F.; Thomas, P. *J. Phys.: Condens. Matter* **1997**, *9*, 2699−2706.
(57) Monroe, D. *Phys. Rev. Lett.* **1985**, *54*, 146−149.
(58) Meijer, E. J.; Tanase, C.; Blom, P. W. M.; van Veenendaal, E.; Huisman, B.-H.; de Leeuw, D. M.; Klapwijk, T. M. *Appl. Phys. Lett.* **2002**, *80*, 3838−3840.
(59) Horowitz, G.; Hajlaoui, M. E.; Hajlaoui, R. *J. Appl. Phys.* **2000**, *87*, 4456−4463.
(60) Dimitrakopoulos, C. D.; Purushothaman, S.; Kymissis, J.; Callegari, A.; Shaw, J. M. *Science* **1999**, *283*, 822−824.
(61) Salleo, A.; Chen, T. W.; Voelkel, A. R.; Wu, Y.; Liu, P.; Ong, B. S.; Street, R. A. *Phys. Rev. B: Condens. Matter* **2004**, *70*, 115311/1−10.
(62) Shur, M.; Hack, M. G.; Shaw, J. G. *J. Appl. Phys.* **1989**, *66*, 3371−3380.
(63) Shur, M.; Hack, M. *J. Appl. Phys.* **1984**, *55*, 3831−3842.
(64) Shur, M.; Hyun, C.; Hack, M. *J. Appl. Phys.* **1986**, *59*, 2488−2497.
(65) Bassler, H. *Phys. Status Solidi B* **1993**, *175*, 15−56.
(66) Arkhipov, V. I.; Heremans, P.; Emelianova, E. V.; Adriaenssens, G. J.; Bassler, H. *Appl. Phys. Lett.* **2003**, *82*, 3245−3247.
(67) Nikitenko, V. R.; Heil, H.; von Seggern, H. *J. Appl. Phys.* **2003**, *94*, 2480−2485.

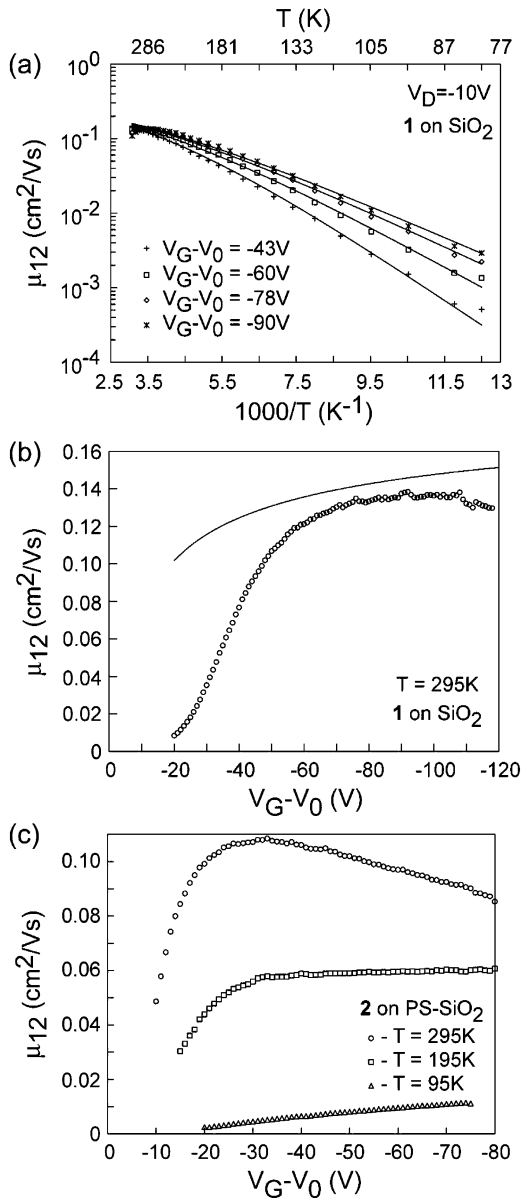

Figure 12. (a) Contact corrected mobility (μ_{12}) versus inverse temperature for several V_G-V_0 values for a TFT based on **1** on SiO_2 ($V_D = -10$ V). The lines represent fits based on the double exponential distribution model. (b) Contact corrected mobility (μ_{12}) versus V_G-V_0 at $T = 295$ K for the same TFT as in part a. The solid line is the attempt to fit (unsuccessfully) the gate-voltage dependence of the mobility based on the fit parameters used in part a. (c) Contact corrected mobility (μ_{12}) versus V_G-V_0 for a film of **2** at several temperatures. The mobility trend is different at each temperature.

2.3×10^{19} cm^{-3}, $E_{dd} = 60$ meV, and $\mu_0 = 0.24$ cm^2/Vs. The trap concentrations equate to 15 shallow traps per 100 molecules and 2 deep traps per 100 molecules of **1**, assuming the traps reside in the first monolayer next to the gate dielectric.

At first glance, the agreement between the calculated mobilities and the data in Figure 12a appears reasonable. However, the limitations of the model begin to appear upon closer inspection of the fit parameters. First, the free carrier mobility (μ_0) is less than experimentally observed values (0.5 cm^2/Vs) for **1** on a different substrate, namely PS−SiO_2. Second, the number of deep traps is about 1 order of magnitude greater than that estimated from the turn-on voltage shift. Third, inspection of Figure 12b shows that the gate-voltage dependence of the mobility at a single temperature is not well predicted. The poor model prediction of the gate-voltage dependence of the mobility is emphasized in Figure 12c, which shows the mobility−gate voltage relationship at several different temperatures for a film of **2** on PS−SiO_2. The same trends were exhibited for contact-corrected and uncorrected mobility values as a function of gate voltage. At room temperature, the mobility increases as function of increasing gate up to a peak and then decreases. The MTR model with a fixed thickness conducting channel is completely unable to predict a decrease in mobility with increasing gate voltage. Thus it was not possible to obtain a reasonable fit to the $T = 295$ K curve in Figure 12c. Interestingly though, the mobility versus gate-voltage behavior in Figure 12c changes with temperature. For example, at the lower temperatures the mobility only exhibits a monotonic increase with gate voltage. We propose these observations can be understood qualitatively in terms of a recent model considering the layered structure of most vapor-deposited organic semiconductors.

It is important to note here that the mobility data in Figure 12 are reported for transistors with negligible hysteresis in the I_D-V_G characteristics. Hysteresis (threshold voltage shift) can lead to an apparent decrease in mobility at high gate voltages, but this possibility can be eliminated for the devices we studied. In addition, the mobility trend was the same at all three drain voltages studied, which eliminates device heating as a possible cause of the mobility versus gate voltage behavior.

Horowitz proposes a model[68] where the semiconductor film is taken as a stack of dielectric layers of thickness d. Using Gauss's law, the induced charge is partitioned among the layers according to

$$\sigma_i = \sigma_{i+1} \exp\left(\frac{1}{kT}\frac{d}{\epsilon_s}\sigma_{i+1}\right) \text{ for } i = 1, n-1 \qquad (9)$$

$$\sum_1^n \sigma_i = \frac{C_{ox}V_G}{e} \qquad (10)$$

where σ_i is the surface charge density of the ith layer and ϵ_s is the dielectric constant of the semiconductor. To understand the implications of the model, we used the values for a film of **2**: $d = 26.97$ Å, $C_{ox} = 11.54$ nF/cm^2, $n = 13$ layers (350 Å film), and we assumed $\epsilon_s = 3\epsilon_0$, where ϵ_0 is the permittivity of vacuum. Figure 13a shows the distribution of induced charge in the first five layers (layer 1 is nearest the gate dielectric) of the film as well as the total induced charge. At low gate voltage, the charge is more evenly distributed over the different layers of the film. With increasing gate voltage, more charge resides in the first layer as seen by the nearly overlapping circles of the first layer and the total induced charge. To examine the effect of temperature on the distribution of charge, the percentage of induced charge in the first layer of the film versus gate voltage for three temperatures is shown in Figure 13b. From the graph, it can be seen that the gate-induced charge is distributed more equally among the layers at higher temperatures. As temperature is decreased, a greater fraction of the induced charge resides in the first layer. Thus, most of the charge resides in the first layer at high gate voltages and low temperatures.

If we assume that the first layer of the film has a lower effective hole mobility than the subsequent layers (due to a

(68) Horowitz, G. *J. Mater. Res.* **2004**, *19*, 1946−1962.

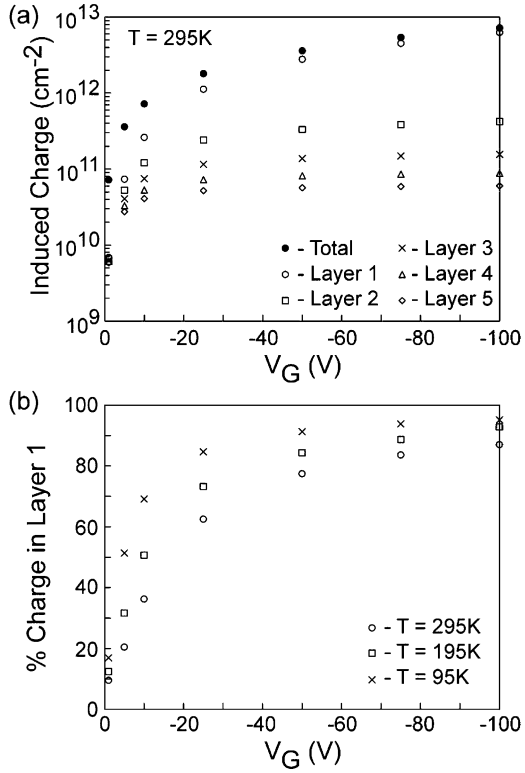

Figure 13. (a) Total induced charge and the induced charge in layers 1−5 as a function of gate voltage at $T = 295$ K using $d = 26.97$ Å, $C_{ox} = 11.54$ nF/cm^2, $n = 13$, and $\epsilon_s = 3\epsilon_0$ in eqs 9 and 10. (b) Percentage of charge in the first layer of the semiconductor film as a function of gate voltage for three temperatures for the Horowitz layer model.[68]

higher concentration of traps), this model can qualitatively explain the trends seen in Figure 12c. The gate-voltage dependence of the mobility is the result of the competition between (1) the distribution of induced charge over multiple layers of the film with different trap densities and different effective mobility values and (2) the gate-induced Fermi level shift toward the mobility edge through the distribution of trap states. The movement of the Fermi level through the trap distribution will lead to an increasing mobility as gate voltage is increased. At the same time, as a larger percentage of the induced charge resides in the first layer with increasing gate voltage, the measured mobility will *decrease* due to the lower effective mobility of the first layer. Thus, the competition between these two effects (charge distribution versus trap filling) can explain a peak in mobility versus gate voltage. In addition, the increased confinement of the charge to the first layer at lower temperatures can lead to a qualitative change in the mobility−gate-voltage dependence. Specifically, at lower temperatures the only important factor is trap filling in the first layer because there is negligible charge in the higher layers. So in this case the mobility would be predicted to simply increase with gate voltage. Figure 12c supports this picture as the gate-voltage dependence of the mobility changes from peaked at $T = 295$ K to a plateau at $T = 195$ K to monotonically increasing with gate voltage at $T = 95$ K. The assumption of a single layer conducting channel becomes better as temperature is decreased. To accurately represent the temperature and gate-voltage dependence of the mobility, a model incorporating the distribution of charge through layers of different effective mobility must be developed.

One way to approach this problem is to make it quasi two-dimensional by considering each layer as separate and not interacting; i.e., charges only travel through one layer from source to drain. In this case, the layers act as parallel resistances between source and drain and the effective mobility of the transistor can be written as

$$\mu_{\text{eff}} = \frac{\sum_{i=1}^{n} \sigma_i \mu_i}{n N_{\text{tot}}} \tag{11}$$

where N_{tot} is the total induced charge, μ_i is the mobility in layer i, and n is the number of layers in the film. σ_i can be determined for each gate voltage using eqs 9 and 10. A distribution of states needs to be assumed for each layer with a corresponding $N_{\text{trap},i}$ (concentration of traps in layer i). For a thirteen layer film, there are 15 adjustable parameters, assuming μ_0 and E_{td} are constant across layers, for a single-exponential distribution in each layer and 29 adjustable parameters for a double exponential distribution with similar assumptions. Once guesses have been made for the adjustable parameters, eq 7 is solved for each layer to get $E_{\text{Fi}}(V_G - V_0, T)$, which is the Fermi level in the ith layer. Once E_{Fi} is known, eqs 5 and 8 can be used to solve for $\mu_i(V_G, T)$. The effective mobility of the transistor can then be calculated from eq 11 and compared to the experimentally measured mobility at each gate voltage and temperature in an iterative scheme. The large number of adjustable parameters makes it unclear precisely how enlightening such a computationally intensive model would be. Yet, in general terms, it is clearly important to understand the physical picture for conduction in organic TFTs, and this justifies attempts to obtain better fits to the gate-voltage and temperature dependence of the mobility.

4. Conclusions

We have reported the structural and electrical characterization of two new p-channel organic semiconductors, 5,5′-bis(2-tetracenyl)-2,2′-bithiophene (**1**) and 5,5′-bis(2-anthracenyl)-2,2′-bithiophene (**2**). Thin films of **1** and **2** exhibited terraced grains with a primary d spacing of 31.83 and 26.97 Å, respectively. Films of **1** and **2** pack in similar triclinic unit cells as determined by GIXD with the long axes of the molecules nearly perpendicular to the substrate. Organic thin-film transistors based on **1** and **2** showed linear regime mobility as high as 0.5 cm^2/Vs and 0.1 cm^2/Vs, respectively. The specific contact resistance, as measured by a four-probe technique, for gold top contacts, was 2×10^4 Ω cm and 3×10^4 Ω cm for **1** and **2**, respectively. Variable temperature measurements revealed activation energies as low as 22 and 27 meV for **1** and **2**, respectively. The temperature and gate-voltage dependence of the mobility were explained within the framework of a double exponential distribution of trap states and a model recognizing the layered structure of the organic films. Importantly, both compounds exhibited a high degree of thermal stability and were more air stable than pentacene. Compound **2** in particular appears to be a promising air stable p-channel organic semiconductor.

Acknowledgment. This work was supported in part by the American Chemical Society Petroleum Research Fund (36589-AC) and the Materials Research Science and Engineering Center at Minnesota (DMR-021302), which is funded by the National

Science Foundation. C.D.F. also thanks 3M Company for financial support of this work.

Supporting Information Available: Explanation of GIXD data analysis and thin-film unit cell parameter calculations, additional thin-film XRD spectra for **2**, GIXD spectrum showing the doublets of **1**, and more details of the double exponential distribution model. This material is available free of charge via the Internet at http://pubs.acs.org.

JA044078H